Journal of Power Sources 204 (2012) 162–167

Contents lists available at SciVerse ScienceDirect

Journal of Power Sources

journal homepage: www.elsevier.com/locate/jpowsour

Nanoscale size effect of titania (anatase) nanotubes with uniform wall thickness as high performance anode for lithium-ion secondary battery

Sovan K. Panda [a], Youngjin Yoon [a], Hyun Suk Jung [b], Won-Sub Yoon [b,*], Hyunjung Shin [a,*]

[a] School of Advanced Materials Engineering, Kookmin University, Seoul 136-702, Republic of Korea
[b] Sungkyunkwan University, Suwon, Gyeonggi-do 440-746, Republic of Korea

ARTICLE INFO

Article history:
Received 7 November 2011
Received in revised form
20 December 2011
Accepted 23 December 2011
Available online 2 January 2012

Keywords:
Titanium dioxide
Nanotubes
Atomic layer deposition
Anode material
Lithium-ion battery

ABSTRACT

We report the synthesis of titania (TiO_2) nanotubes (NTs) with precisely controlled wall thickness by atomic layer deposition (ALD) using alumina membranes as template and their application as anode material for lithium (Li) ion storage in secondary battery. As-grown nanotubes are amorphous in nature and transform into anatase phase by subsequent thermal annealing. The charge/discharge capacities and rate performance are found to be dependent on the wall thickness, which is highly uniform, of the NTs. Maximum reversible capacity for Li-insertion in anatase $TiO_2 \sim 330\,mAh\,g^{-1}$ has been achieved by reducing the tube wall thickness to 5 nm. NTs with the wall thickness of 40 nm show reversible capacity of $\sim 170\,mAh\,g^{-1}$ which is similar to the maximum theoretical capacity of the bulk anatase as reported. With decrease in the wall thickness, rate performance of the NTs is significantly improved. NTs with 5 nm in the wall thickness render excellent rate capability and cycle response.

1. Introduction

Materials for electrode often play a vital role in the development of new generation of lithium-ion batteries with improved cell performance. The search for novel electrode materials with enhanced electrochemical properties as well as safer and cheaper is still remains a challenge. As a challenge to improve the cell performance of Li-storage, nanostructuring is promising scheme which enables higher intercalation/de-intercalation rates and power [1–3]. The reduced dimensions significantly diminish the ionic and electronic paths and provide a very high surface area, which improves the rate capability and specific capacity. Li-ion batteries using nanoparticle-based electrodes have been reported in the literature, which show better performance compared to their bulk and/or thin films [4–7]. The main drawback using the nanoparticle-based electrodes is identified with their long current flow path and hence slow charging/discharging rate. Vertically aligned array of the one-dimensional (1D) nanostructures (NSs), for example, nanorods, nanowires, nanotubes (NTs), etc., directly on metallic substrates as current collectors are expected to have some more advantages, which include larger surface area, efficient diffusion of electrolyte, accommodation of strain without irregular expansion and directional pathway of carriers, over the nanoparticle-based electrode [8,9]. Among 1D NSs, NTs are superior to nanorods and nanowires as electrode materials on the account of their higher surface area (both the inner and outer surfaces can be exposed to the electrolyte) which is beneficial for electrochemical performance [10–15]. Axial void spaces of the NTs also accommodate the volume expansion during Li-insertion and extraction and eliminate the internal stress in the material providing excellent cyclability [16].

TiO_2 has been studied extensively as anode material for Li-ion battery since it has very high chemical stability, low self-discharge rate, low fabrication cost and environmentally benign. TiO_2 has been recognized as a safe anode material owing to its higher Li-insertion potential ($\sim$1.7 V vs Li^+/Li) compared to well known graphite anode ($\sim$0.1 V vs Li^+/Li). Electrochemical performance of various TiO_2 phases including anatase ($I4_1/amd$) [17–19], rutile ($P4_2/mnm$) [20,21], TiO_2-B ($C2/m$) [22], brookite ($Pbca$) [23], hollandite ($I4/m$) [24], ramsdellite ($Pbnm$) [25] and amorphous [26,27] have been investigated. Among them, anatase is remarkable of its reversible uptake of 0.5 Li per TiO_2 formula unit [28] and fast Li-ion insertion and extraction for which high power and energy densities can be expected. The overall Li insertion and de-insertion in/from the TiO_2 can be described as:

$$TiO_2 + xLi^+ + xe^- \leftrightarrow Li_xTiO_2 \quad (1)$$

Upon Li insertion, the tetragonal phase TiO_2 (space group: $I4_1/amd$) undergoes a phase transition to orthorhombic lithium titanate

* Corresponding authors. Tel.: +82 2 910 4897; fax: +82 2 910 4320.
E-mail addresses: wsyoon@skku.edu (W.-S. Yoon), hjshin@kookmin.ac.kr (H. Shin).

0378-7753/$ – see front matter © 2012 Elsevier B.V. All rights reserved.
doi:10.1016/j.jpowsour.2011.12.048

($Li_{0.5}TiO_2$, space group: *Imma*) through Li-poor TiO_2 solid solutions (space group: $I4_1/amd$) [29,30]. The transformation from anatase to $Li_{0.5}TiO_2$ orthorhombic phase is a completely reversible reaction. The inserted Li-ions in the TiO_2 matrix occupy the interstitial octahedral sites in random fashion where there are four octahedral sites available per unit cell. The average overall occupation factor of the octahedral sites of anatase (~0.5) is restricted by the Li^+–Li^+ repulsive interactions. The main redox reaction responsible for the electrochemical activity is the conversion of Ti^{4+}/Ti^{3+} during the discharge process and vice versa during the charging process.

It has been reported that the nanosized TiO_2 can accept more Li in the structure forming a new phase Li_1TiO_2 having the same space group ($I4_1/amd$) as anatase, but with shifted lattice parameters *a*, from 3.792 to 4.043 Å and *b*, from 9.497 to 8.628 Å [31]. With the formation of Li_1TiO_2 ($x = 1$) phase, the structure hosts extra Li compared to the bulk and the capacity reaches to the theoretical maximum value of ~335 mAh g^{-1} for the anatase TiO_2. The particle sizes below 7 nm can only hosts lithium fraction $x = 1$ and completely converts into Li_1TiO_2, whereas larger particles convert less and makes the maximum obtainable Li fraction depending on the particle size [32–34]. Using particles in nanometer scale, it has inherently the size distribution and makes the conclusion unclear. Therefore, size-controlled as well as mono-sized 1D NSs (diameter in the case of nanowires and/or nanorods and wall thickness in NTs) of TiO_2 are ideal candidate to maximize the performances and to study the "true" nanoscale size effect in Li intercalations.

Most of the TiO_2 NT array based anodes for lithium-ion battery application have been grown directly on Ti metal by anodic oxidation taking the advantage of the conductivity of the metal sheet which takes part as current collector. Precise control of wall thickness of the NTs in nanometer range accuracy by anodic oxidation is, however, a nontrivial task. Atomic layer deposition (ALD) is superb in this respect because of its self-limiting nature, which gives rise to a conformal growth over high aspect ratio features and an easy control over the wall thickness of NTs. In spite of these remarkable features, ALD grown TiO_2 NTs have attracted a little attention so far for electrode (anode) application in Li-ion battery [35] because of the product cost point of view. Although anodization of Ti metal is simpler and inexpensive than ALD, anodization is not suitable to study precisely the wall thickness dependent electrochemical performance of the NTs owing to the lack of control over the structure and growth rate. Here in, we have applied ALD for the synthesis of TiO_2 NTs using porous alumina membrane as template where the current collector was fabricated by depositing the Ti metal film on one face of the NTs. In this paper, we have reported the electrochemical performance of arrayed TiO_2 NT-based anodes with the variations in the wall thickness of the tubes. The "true" nano-size effect in mono-sized tubular structure for the hosting of Li-ions has been discussed.

2. Experimental

Arrays of TiO_2 NTs were fabricated by coating the inner pores of commercially available alumina membranes (Anodisk 13, Whatman, UK) by atomic layer deposition (ALD) (Ozone-Forall, Korea) using titanium (IV) iso-propoxide (TTIP, UP Chemical) as Ti precursor and water vapor as oxidant. Ar gas with flow rate of 100 sccm was used as carrier and also for purging. Single ALD cycle consisted of an injection of TTIP for 10 s, an Ar purge for 40 s, H_2O vapor pulse for 10 s, and another Ar purge for 40 s. All the depositions were performed at 160 °C with a working pressure of ~347 N m^{-2}. After completion of each cycle, the chamber was evacuated by a rotary pump in order to remove the excess reactants and the reaction by-products. Total time required for the completion of each cycle was 100 s. Alumina membranes were mounted on a Si wafer in a bridge like geometry (supported from the two side bottoms and hanging the membrane over the supports) so that the vapor species can enter through both the top and bottom faces of the pores to guarantee conformal coatings. TiO_2 deposition rate was found to be approximately 0.33 Å per cycle. To fabricate TiO_2 NTs with the wall thicknesses of 2, 5, 20 and 40 nm, ALD cycles of 60, 150, 600 and 1200, respectively, were carried out. As-grown TiO_2 coated alumina membranes were then annealed at 400 °C in air for 1 h in a box furnace.

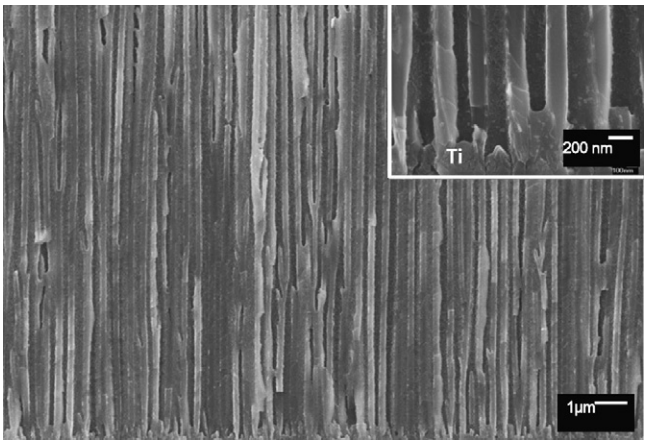

Fig. 1. Cross-sectional FESEM image of TiO_2 NTs inside alumina template. Inset shows the cross-sectional FESEM image of Ti thin film deposited at one face of the NTs.

The structural and morphological properties of the TiO_2 NTs were characterized by X-ray diffraction (XRD), transmission electron microscopy (TEM) and scanning electron microscopy (SEM). XRD patterns were recorded with θ–2θ configuration by Philips X'pert system using Cu Kα radiation. The morphology of NTs was observed by JEOL JMS-7401F scanning electron microscope (SEM). A JEOL-FEM 4010 transmission electron microscope (TEM) operating at 400 kV was used to obtain TEM and HRTEM images of the NTs. For TEM, samples were prepared by dissolving the alumina membrane in 1 M aqueous NaOH solution and dispersing the NTs ultrasonically in de-ionized water and dropping the dispersed solution on a carbon coated copper grid.

All electrochemical measurements were performed using two-electrode cells. Galvanostatic cycling tests were performed using TiO_2 NTs as working electrodes. As current collector, we deposited Ti metal by e-beam evaporation onto the NTs which were supported by alumina membranes. Li metal was used as the counter electrode. Glass micro fibers (Whatman, UK) were used as separators. Electrolyte was a solution of 1 M lithium hexafluorophosphate ($LiPF_6$) in 1:1 mixture of ethylene carbonate and dimethyl carbonate. No binders or conducting carbon were used. Cell assembly was carried out in an Ar-filled glove box and packed into a coin cell. The cells were galvanostatically cycled using a Won A Tech WBCS 3000 system and measuring potential was in a potential range of 0.7–3.0 V (Li^+/Li) at current rates from the C/10 to 1785 C (1 C ≡ one lithium per formula unit in 1 h). The mass of TiO_2 NTs was measured directly using a microbalance (XR205SM-DR, with precision of 10 μg).

3. Results and discussion

Porous alumina templates used have an average pore diameter of ~200 nm, channel length of ~60 μm with aspect ratio of ~300 and pore density of ~10^9 cm^{-2}. Cross-sectional FE-SEM image of the well ordered NT array inside the AAO membrane is shown in Fig. 1. The shape of the NTs is exactly the same as the pores

(~200 nm outer diameter and ~60 μm in length) in the templates. The templates were not removed after ALD cycles, which provide mechanical support to the NTs and make them easy in handling. The alumina barrier between the NTs further acts as a proactive structural buffer against the agglomeration of NTs. Inset of Fig. 1 illustrates the cross-sectional FE-SEM image of the deposited Ti thin film on one face of the NTs, which acts as current collector. Since the NTs are directly connected to the current collector, electrons can be quickly transferred from the redox site to the collector through an efficient way without using external conducting particles and/or binders which is of great significance to enhance the rate capability of the anode material. XRD pattern of the as-deposited NT array (Fig. 2a) with 20 nm tube wall thickness inside the alumina template doesn't show any diffraction peak (except one around $2\theta = 38^\circ$ corresponds to the main peak from the e-beam evaporated Ti (0 0 2) metal layers as current collectors) corresponding to crystalline TiO_2 phases in the diffraction pattern of as-deposited NTs which indicates that the as-grown NTs are amorphous. Annealed NTs show diffraction peaks corresponding to anatase (TiO_2) phase with lattice constants of $a = 3.785$ Å and $c = 9.513$ Å (JCPDS card No. 211272). Annealing of the NTs at 400 °C in air for 1 h leads to a transformation from amorphous to tetragonal anatase phase [36]. The sharp and intense diffraction peaks in the XRD pattern of the 20 nm in the thickness of NTs indicate complete crystallization containing large enough grains. As expected, line-width of the diffractions increases for 5 nm in thickness of NTs as a result of small crystals' size broadening. From bright field TEM images of Fig. 2b, the obtained average wall thicknesses are ~5, 20 and 40 nm which are corresponding to the 150, 600 and 1200 cycles of ALD, confirming almost constant growth rate of ~0.33 Å per cycle. TEM images further prove that the average outer diameter of the NTs is ~200 nm which is the same as the average pore diameter of the alumina template and the pores are almost conformally coated by TiO_2. Selected area electron diffraction (SAED) patterns reveal that the NTs are anatase TiO_2, which is consistent with the XRD results. ALD is the method that can meet the high demands of structural parameters including the diameter, length and wall thickness [37–40].

Fig. 3a demonstrates the electrochemical performances of anatase TiO_2 NT based anodes with the function of the wall thicknesses in galvanostatic mode using a C/10 current rate between 3.0 and 0.7 V. Array of NTs with the wall thicknesses of 2, 5, 20 and 40 nm was used as anodes for the present study. The shape of the charge and discharge curves is in well agreement with the previous reports on TiO_2 NT, nanorod and nanoparticle based anodes where the discharging and charging plateaus were appeared at ~1.7 V and ~1.8 V, respectively [15,32,41,42]. The discharge curves of the present study can be classified into three zones: a sharp decrease in potential (above ~1.70 V), a plateau region (at ~1.70 V) and a continuous sloped region (below ~1.60 V). The plateau region in the charging curve appears above 1.80 V, which is at higher potential compared to the discharge plateau (~1.70 V). This fact suggests that the Li intercalation in TiO_2 matrix arises at lower potential than the de-intercalation. The Li insertion above ~1.70 V (i.e., initial monotonous potential decrease region) in the discharge curve is caused by the formation of a solid solution [32]. The insertion of Li-ions in this region does not cause any structural change and create a Li-poor phase with the same space group ($I4_1/amd$) as anatase. It is noted that the capacity related to the solid solution regions have been reduced in the second discharge curves compared to the first discharge, which occurs due to the irreversible capacity caused by the solid-electrolyte interphase (SEI) formation in the first cycle. This SEI formation is permanent and the corresponding capacity is lost during the first discharge cycle, which takes part in the large irreversible capacity. The appearance of the flat plateau in the charge/discharge curve denotes phase equilibrium between anatase TiO_2 and Li_xTiO_2 ($x = 0.5$) within which half of Ti^{4+} is converted to Ti^{3+} along with the insertion of Li ions [43]. In this region, Li insertion into the interstitial octahedral sites of the anatase crystal takes place. As a result, a phase transformation from tetragonal to orthorhombic is observed leading to $Li_{0.5}TiO_2$ with the expense of anatase phase. The capacity corresponding to this plateau region is almost reversible. A large part of the discharge curves is made of a long slope region (<1.60 V), which mainly occurs due to the surface effects. The sloped region is formed by the additional insertion of the Li ions into the surface layer under the

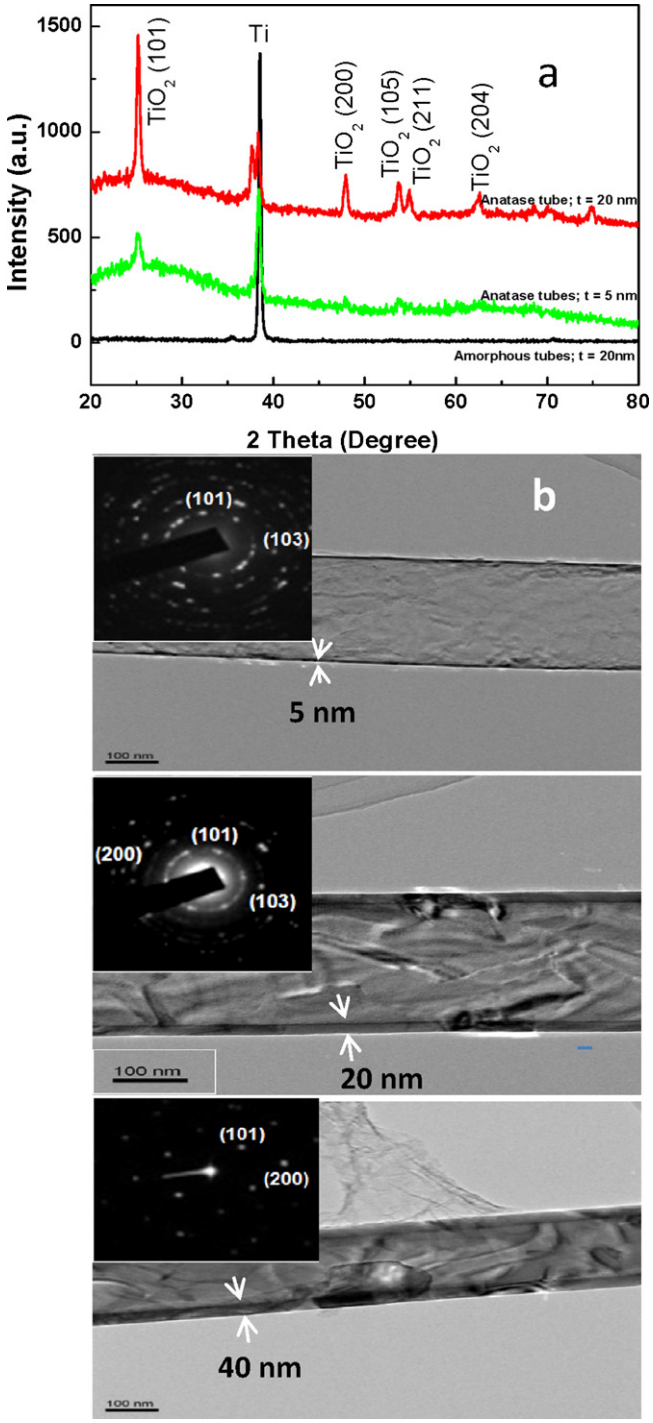

Fig. 2. (a) XRD θ–2θ scan of as-deposited (wall thickness $t = 20$ nm) and annealed (5 nm and 20 nm wall thickness) NTs (b) TEM images of annealed (anatase) NTs with wall thicknesses: 5 nm, 20 nm, 40 nm. Insets show the SAED patterns corresponding to the NTs.

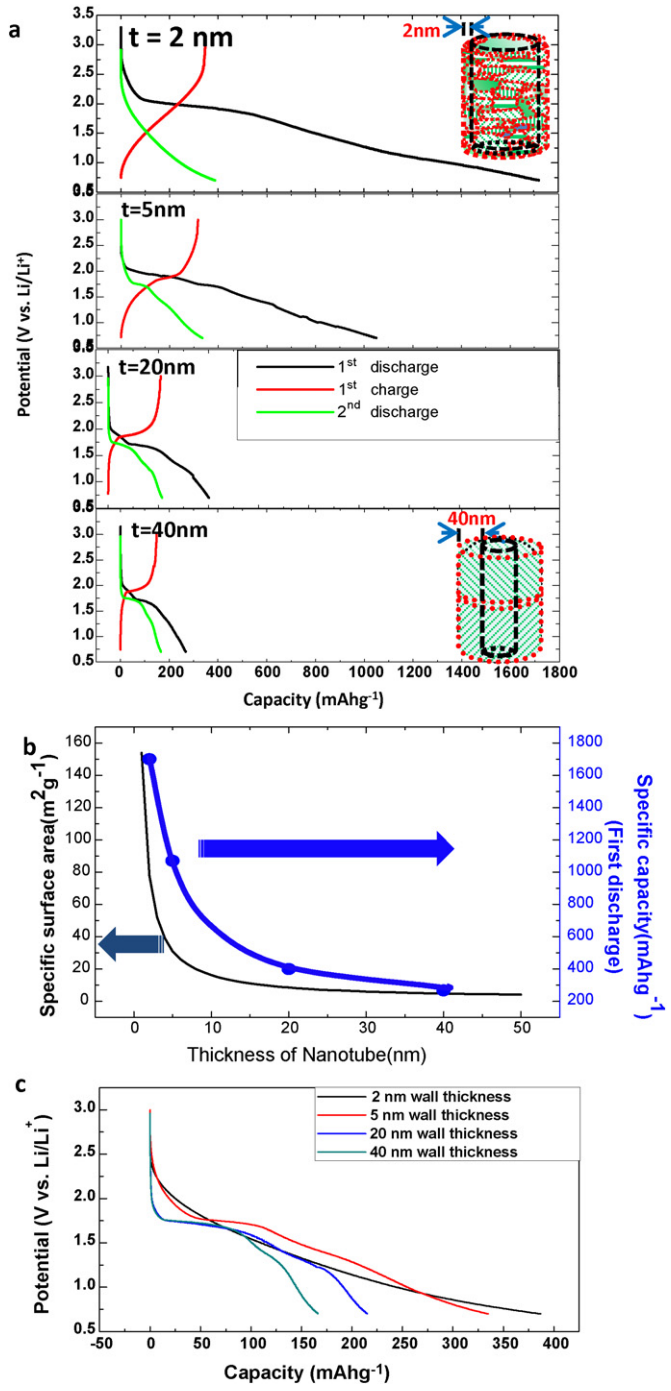

Fig. 3. (a) Electrochemical performance of anatase TiO_2 NTs with 2, 5, 20 and 40 nm wall thicknesses as anode in galvanostatic mode using a C/10 current rate. (b) Plot of specific surface area and specific capacity of NT-based anodes with various wall thicknesses. (c) Plot of second discharge curves for various tube wall thicknesses.

external force of the electric field after the filling up of all available interstitial octahedral sites. Since the nanomaterials have very high surface to volume ratio, the role of this region is prominent compared to the bulk.

The discharge and charge capacities are found to increase with decrease in the wall thickness. First discharge capacities for 40, 20, 5 and 2 nm thick NTs are around 270 ($x \sim 0.8$), 400 ($x \sim 1.2$), 1050 ($x \sim 3.1$) and 1700 mAh g^{-1} ($x \sim 5.2$), respectively. The capacities in the second discharge (reversible) are decreased to 170 ($x \sim 0.5$), 220 ($x \sim 0.7$), 330 ($x \sim 1.0$) and 400 mAh g^{-1} ($x \sim 1.2$), for 40, 20, 5 and 2 nm thick NT anodes, respectively. The corresponding irreversible capacity loss for NT-based anodes are ~100 ($x \sim 0.3$), 180 ($x \sim 0.5$), 720 ($x \sim 2.2$) and 1300 mAh g^{-1} ($x \sim 4.0$) for the wall thicknesses of 40, 20, 5 and 2 nm, respectively. Table 1 summarizes all the reversible and irreversible capacities obtained from the 1st and 2nd discharging of the NT array for different wall thicknesses. The reversible specific capacity of the 40 nm thick NT-based anode is similar to the capacity for bulk anatase TiO_2 (~168 mAh g^{-1}) [28]. For 20 nm thick NTs, the reversible specific capacity became ~220 mAh g^{-1} leaving an irreversible capacity loss ~180 mAh g^{-1}. Therefore, reversible capacity increases with decrease in the wall thickness and reaches to 330 mAh g^{-1} ($x \sim 1$) for 5 nm thick NTs. This phenomenon is similar to the TiO_2 nanoparticles reported recently where the capacity reaches to the maximum theoretical value of 335 mAh g^{-1} ($x = 1$) below the particles' mean diameter of 7 nm [31,32]. Maximum value of lithium fraction (x) in Li_xTiO_2 should be 1 for pure crystalline phase. In the present study, the value of x has been exceeded 1 which results from the very large specific surface area, small wall thicknesses of the NTs and imperfections in the crystals. Also the main effect of increasing surface area is to broaden the energy levels accessible to materials, and thus leading to a voltage distribution at which the electrochemical reaction takes place. The correlation between specific surface area and capacity of nanostructured materials has been previously observed in mesoporous TiO_2 and nanoparticles [44]. As a result, the first discharge capacities for 2 and 5 nm thick NTs are outstanding and observed for the first time using anatase TiO_2. The specific surface area of NT-based anodes have been calculated (considering only the inner surface of the tubes because the outer surface is covered by alumina templates) and plotted with the wall thicknesses, which is shown in Fig. 3b. Specific surface area and the first discharge specific capacities of the NT anodes are found to increase exponentially with the reduction of the wall thicknesses. For 2 nm wall thickness, the surface area reaches to a maximum ~150 m^2 g^{-1} and reduces to ~10 m^2 g^{-1} for 40 nm in the wall thickness. The increased surface area can inevitably increase the proportion of the total numbers of atoms lie near or on the surface and subsequently increase the intercalation of Li on or near the surface. Since the sloped region of the discharge curve (<1.60 V) mainly represents the intercalation of Li ions at the surface, the length of this region should increase with decrease in tube wall thickness. The results are also consistent with this argument. The length of the slope region is maximum for 2 nm NTs and minimum for 40 nm NTs. It has been reported that the Li ions inserted in the surface layers are highly reversible except those are trapped in the initial insertion because of dangling bonds and surface disordering [43]. Increase in the specific surface area may increase the initial trapping probability of Li ions on the surface, which results large irreversible capacity with decrease in the wall thickness. The large irreversible capacity may results from the reaction between adsorbed water molecules on the NTs and Li-ions by the following reaction [42]:

$$H_2O + Li^+ + xe^- \leftrightarrow Li_xOH + \tfrac{1}{2}H_2 \quad (2)$$

The water adsorption onto the NTs is proportional to the surface area. Therefore, the 2 and 5 nm thick NTs have large specific surface area and should have absorbed large amount of water molecules, which may lead the reaction between water and Li-ions and produce large irreversible capacity. This reaction rate is not much significant in the case of 20 and 40 nm thick NTs due to their relatively low specific surface area. Upon subsequent cycling, irreversible capacity is not observed, indicating that water have been completely consumed during the first discharging process.

The bi-phasic plateau region is also dependent on the NT wall thickness. The length of the plateau region at ~1.70 V becomes less resolved with decreasing thickness of TiO_2 NTs. Shortening of plateau region is also thought to be related to the increase in specific surface area. Li intercalation in nanostructured anatase

Table 1
Reversible and irreversible capacities obtained from the 1st and 2nd discharging of the TiO_2 NT array based anodes with 2, 5, 20 and 40 nm wall thicknesses.

Tube wall thickness (t) (nm)	1st discharging		2nd discharging (reversible)		Irreversible	
	Capacity (mAh g^{-1})	Lithium fraction (x)	Capacity (mAh g^{-1})	Lithium fraction (x)	Capacity (mAh g^{-1})	Lithium fraction (x)
2	1700	5.2	400	1.2	1300	4.0
5	1050	3.1	330	1.0	720	2.2
20	400	1.2	220	0.7	180	0.5
40	270	0.8	170	0.5	100	0.3

electrode occurs in both the surface and bulk region. As the wall thickness reduces, the surface area plays dominant role in Li intercalation because the interstitial octahedral sites decrease due to the increase in total number of atoms on the surface. Therefore, larger the surface area means large number of atoms on the surface and lesser the octahedral sites for Li-intercalation and hence the length of the plateau region reduces. In the second discharge curve for 2 nm thick TiO_2 NTs, the bi-phasic region has almost been eliminated and the discharge curve looks similar to amorphous TiO_2 anode. This is because of very thin wall thickness, which may suppress the octahedral sites and hosts Li ions mostly on the surfaces. The solid solution region of the charge/discharge curve (initial monotonous potential decrease >1.70 V) also depends on the wall thickness of the NTs. Nanoparticles (mean diameter of ~6 nm) can host up to $x = 0.22$ Li fraction while maintaining the anatase structure [17]. It has been further reported that the TiO_2 nanoparticles with diameter 120 nm and 7 nm can host 0.03 and 0.21 Li fractions, respectively [31]. Therefore, the value of Li fraction in the solid solutions increases with decrease in size. In our present study, we have also observed the increase in length of the solid solution region with decrease in the NTs' wall thicknesses (Fig. 3c). The solid solution region for 40 and 20 nm thick NTs are almost identical but the capacity corresponding to this region is highest for 2 nm one followed by 5 nm NTs. The phase diagram for Li and TiO_2 also suggests that the solid solubility of Li in anatase TiO_2 increases with the reduction of particle size [31].

Rate capability plot of the TiO_2 NT-based anodes for various wall thicknesses (Fig. 4) represents the significant improvement of the rate performance with decrease in the wall thickness up to 5 nm. Specific capacities for 5, 20 and 40 nm NT-based anodes at 1 C current rate are ~250, 140 and 90 mAh g^{-1}, respectively. Maximum C-rate achieved for 5, 20 and 40 nm NT-based anodes are 1785 C, 60 C and 10 C, respectively, before the cells electrically collapse. At faster charging/discharging rate, Li intercalation/de-intercalation

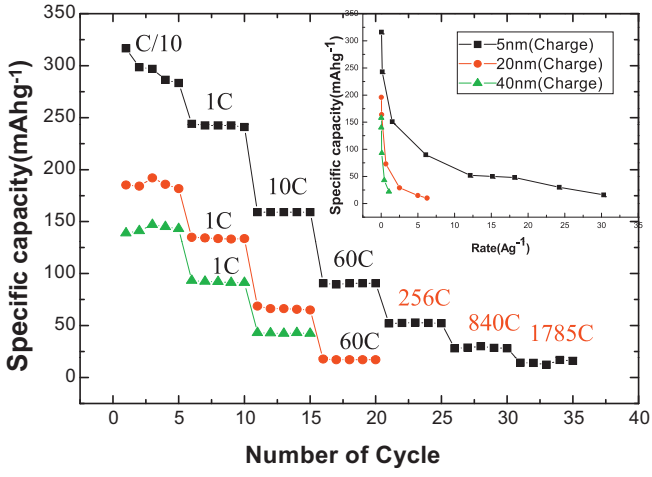

Fig. 4. Rate capability of the TiO_2 NT-based anodes for various tube wall thicknesses. Inset shows the current density dependence of the specific capacity.

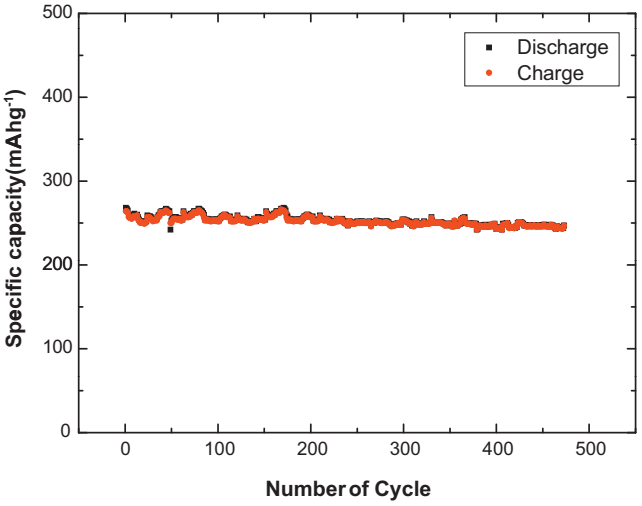

Fig. 5. Cycle response curve for the 5 nm thick NT anode at 1 C current rate.

only occurs near the surface of the NTs because of the very short diffusion time. Due to the shorter Li-diffusion length, most of the interstitial octahedral sites, which remain deeper are still unoccupied by Li-ions in the very short diffusion time. In case of 5 nm thick NTs, specific surface area is higher compared to 20 and 40 nm NTs and most of the atoms lie near to the surface where mainly intercalation takes place. Because of this large surface area, 5 nm thick NT-based anodes can respond faster and show better rate performance compared to 20 and 40 nm NTs. Whereas, the Li-ion insertion mainly takes place into the octahedral sites rather than the surface in 20 and 40 nm NTs. A considerable amount of time is required to diffuse the Li-ions into the deeper octahedral sites. Therefore, a slow charging/discharging rate is preferred for complete filling up the unit cells with Li-ions for thicker NTs which render poor rate performance.

NT-array based anode with the wall thickness of 5 nm shows best performance in term of reversible specific capacity and rate capability compared to the others. Therefore, 5 nm wall thickness NT-array as an anode is expected to yield an excellent cyclability. The cycle performance curve of Fig. 5 represents excellent flat behavior even after 500 cycles. The charge and discharge capacity after 500 cycles is ~250 mAh g^{-1} which is corresponding to ~0.70 Li per TiO_2. The capacity after 5th cycle is ~260 mAh g^{-1}. Therefore, ~95% capacity retention from the 5th cycle is observed after 500 cycles which is outstanding for TiO_2 NT-based anodes. The excellent specific capacity, high rate capacity and cyclability render 5 nm in wall thickness anatase NT-array a promising anode material for Li-ion battery for high power and high energy density applications.

4. Summary and conclusions

In summary, TiO_2 NTs with precisely controlled wall thickness have been grown successfully by ALD using anodic alumina membrane as template. The performance of the Li-ion cells strongly

depend on the wall thickness of the NT-based anode. Both the reversible and irreversible capacities increase with decrease in NTs' wall thickness. With decrease in wall thickness, rate performance also improves significantly. NTs with wall thickness 5 nm show excellent performance in term of specific capacity (330 mAh g^{-1}, $x \sim 1$, at C/10 current rate), rate capability [250 mAh g^{-1} ($x \sim 0.70$) at 1 C, 90 mAh g^{-1} ($x \sim 0.30$) at 60 C] and cyclability (capacity retention: 250 mAh g^{-1} after 500 cycles). Therefore, 5 nm anatase NTs are promising anode material for Li-ion battery for high power and high energy density applications.

Acknowledgments

This work was supported by the National Research Foundation of Korea Grant funded by the Korean Government (MEST) (NRF-2010-0028972; NRF-C1AAA001-2010-0029065). This work was in part supported by the 2011 Research Program of Kookmin University.

References

[1] P.G. Bruce, B. Scrosati, J.-M. Tarascon, Angew. Chem. Int. Ed. 47 (2008) 2930–2946.
[2] M.G. Kim, J. Cho, Adv. Funct. Mater. 19 (2009) 1497–1514.
[3] K.T. Lee, J. Cho, Nanotoday 6 (2011) 28–41.
[4] H. Kim, M. Seo, M.-H. Park, J. Cho, Angew. Chem. Int. Ed. 49 (2010) 2146–2149.
[5] N. Li, C.R. Martin, J. Electrochem. Soc. 148 (2001) A164–A170.
[6] C. Kim, M. Noh, M. Choi, J. Cho, B. Park, Chem. Mater. 17 (2005) 3297–3301.
[7] S.W. Oh, S.-H. Park, Y.-K. Sun, J. Power Sources 161 (2006) 1314–1318.
[8] C.K. Chan, H. Peng, G. Liu, K. Mc Ilwrath, X.F. Zhang, R.A. Huggins, Y. Cui, Nat. Nanotechnol. 3 (2008) 31–35.
[9] Y. Li, B. Tan, Y. Wu, Nano Lett. 8 (2008) 265–270.
[10] Z. Wei, Z. Liu, R. Jiang, C. Bian, T. Huang, A. Yu, J. Solid State Electrochem. 14 (2010) 1045–1050.
[11] K. Wang, M. Wei, M.A. Morris, H. Zhou, J.D. Holmes, Adv. Mater. 19 (2007) 3016–3020.
[12] H. Zhang, X.P. Gao, G.P. Li, T.Y. Yan, H.Y. Zhu, Electrochim. Acta 53 (2008) 7061–7068.
[13] Y. Wang, K. Takahashi, H. Shang, G. Cao, J. Phys. Chem. B 109 (2005) 3085–3988.
[14] M.-H. Park, M.G. Kim, J. Joo, K. Kim, J. Kim, S. Ahn, Y. Cui, J. Cho, Nano Lett. 9 (2009) 3844–3847.
[15] J. Kim, J. Cho, J. Electrochem. Soc. 154 (2007) A542–A546.
[16] T. Song, J. Xia, J.-H. Lee, D.H. Lee, M.-S. Kwon, J.-M. Choi, J. Wu, S.K. Doo, H. Chang, W.I. Park, D.S. Zang, H. Kim, Y. Huang, K.-C. Hwang, J.A. Rogers, U. Paik, Nano Lett. 10 (2010) 1710–1716.
[17] G. Sudant, E. Baudrin, D. Larcher, J.-M. Tarascon, J. Mater. Chem. 15 (2005) 1263–1269.
[18] V. Subramanian, A. Karki, K.I. Gnanasekar, F.P. Eddy, B. Rambabu, J. Power Sources 159 (2006) 186–192.
[19] L. Kavan, M. Gräizel, J. Rathousky, A. Zukal, J. Electrochem. Soc. 143 (1996) 394–400.
[20] N.A. Milne, M. Skyllas-Kazacos, V. Luca, J. Phys. Chem. C 113 (2009) 12983–12995.
[21] Y.-S. Hu, L. Kienle, Y.-G. Guo, J. Maier, Adv. Mater. 18 (2006) 1421–1426.
[22] G. Armstrong, A.R. Armstrong, P.G. Bruce, P. Reale, B. Scrosati, Adv. Mater. 18 (2006) 2597–2600.
[23] M.A. Reddy, M.S. Kishore, V. Pralong, U.V. Varadaraju, B. Raveau, Electrochem. Solid-State Lett. 10 (2007) A29–A31.
[24] L.D. Naoilles, C.S. Johnson, J.T. Vaughey, M.M. Thackeray, J. Power Sources 81–82 (1999) 259–263.
[25] M.V. Koudriachova, Chem. Phys. Lett. 458 (2008) 108–112.
[26] M. Hibino, K. Abe, M. Mochizuki, M. Miyayama, J. Power Sources 126 (2004) 139–143.
[27] H.-T. Fang, M. Liu, D.-W. Wang, T. Sun, D.-S. Guan, F. Li, J. Zhou, T.-K. Sham, H.-M. Cheng, Nanotechnology 20 (2009) 1–7, 225701.
[28] H. Lindstrom, S. Sodergrem, A. Solbrand, H. Rensmo, J. Hjelm, A. Hagfeldt, S.E. Lindquist, J. Phys. Chem. B 101 (1997) 7717–7722.
[29] R. van de Krol, A. Goossens, E.A. Meulenkamp, J. Electrochem. Soc. 146 (1999) 3150–3154.
[30] L.J. Hardwick, M. Holzapfel, P. Novak, L. Dupont, E. Baudrin, Electrochim. Acta 52 (2007) 5357–5367.
[31] M. Wagemaker, W.J.H. Borghols, F.M. Mulder, J. Am. Chem. Soc. 129 (2007) 4323–4327.
[32] U. Lafont, D. Carta, G. Mountjoy, A.V. Chadwick, E.M. Kelder, J. Phys. Chem. C 114 (2010) 1372–1378.
[33] M. Wagemaker, W.J.H. Borghols, E.R.H. van Eck, A.P.M. Kentgens, G.J. Kearley, F.M. Mulder, Chem. Eur. J. 13 (2007) 2023–2028.
[34] M. Wagemaker, A.P.M. Kentgens, F.M. Mulder, Nature 418 (2002) 397–399.
[35] C. Bae, Y. Yoon, W.-S. Yoon, J. Moon, J. Kim, H. Shin, Appl. Mater. Interface 2 (2010) 1581–1587.
[36] A. Jaroenworaluck, D. Regonini, C.R. Bowen, R. Stevens, Appl. Surf. Sci. 256 (2010) 2672–2679.
[37] H. Shin, D.K. Jeong, J. Lee, M.M. Sung, J. Kim, Adv. Mater. 16 (2004) 1197–1200.
[38] C. Bae, S. Kim, B. Ahn, J. Kim, M.M. Sung, H. Shin, J. Mater. Chem. 18 (2008) 1362–1367.
[39] L.K. Tan, M.A.S. Chong, H. Gao, J. Phys. Chem. C 112 (2008) 69–73.
[40] M.S. Sander, M.J. Cote, W. Gu, B.M. Kile, C.P. Tripp, Adv. Mater. 16 (2004) 2052–2057.
[41] J. Xu, C. Jia, B. Cao, W.F. Zhang, Electrochim. Acta 52 (2007) 8044–8047.
[42] G.F. Ortiz, I. Hanzu, T. Djenizian, P. Lavela, J.L. Tirado, P. Knauth, Chem. Mater. 21 (2009) 63–67.
[43] C. Jiang, M. Wei, Z. Qi, T. Kudo, I. Honma, H. Zhou, J. Power Sources 166 (2007) 239–243.
[44] H.S. Zhou, D.L. Li, M. Hibino, I. Honma, Angew. Chem. Int. Ed. 44 (2005) 797–802.